Synthesis, Crystal Structure, EXAFS, and Magnetic Properties of Catena [μ-Tris(1,2-bis(tetrazol-1-yl)propane-*N*1,*N*1′)iron(II)] Bis(perchlorate). First Crystal Structure of an Iron(II) Spin-Crossover Chain Compound

Petra J. van Koningsbruggen,[†] Yann Garcia,[†] Olivier Kahn,[‡] Léopold Fournès,[‡] Huub Kooijman,[§] Anthony L. Spek,[§] Jaap G. Haasnoot,[||] Jacques Moscovici,[⊥] Karine Provost,[⊥] Alain Michalowicz,[⊥,▽] Franz Renz,[†] and Philipp Gütlich*[,†]

Institut für Anorganische Chemie und Analytische Chemie, Johannes Gutenberg University, Staudingerweg 9, D-55099 Mainz, Germany, Laboratoire des Sciences Moléculaires, Institut de Chimie de la Matière Condensée de Bordeaux, UPR CNRS no. 9048, Avenue du Docteur Schweitzer, F-33608 Pessac, France, Bijvoet Center for Biomolecular Research, Crystal and Structural Chemistry, Utrecht University, Padualaan 8, 3584 CH Utrecht, The Netherlands, Leiden Institute of Chemistry, Gorlaeus Laboratories, Leiden University, P.O. Box 9502, 2300 RA Leiden, The Netherlands, Groupe de Physique des Milieux Denses, Université Paris XII-Val de Marne, Avenue du Général De Gaulle, 94010 Créteil Cedex, France, and Laboratoire d'Utilisation du Rayonnement Electromagnétique, Université Paris Sud, Bat 209 D, 91405 Orsay Cedex, France

Received September 20, 1999

$[Fe(btzp)_3](ClO_4)_2$ (btzp = 1,2-bis(tetrazol-1-yl)propane) represents the first structurally characterized Fe(II) linear chain compound exhibiting thermal spin crossover. It shows a very gradual spin transition ($T_{1/2}$ = 130 K) which has been followed by magnetic susceptibility measurements and ^{57}Fe Mössbauer spectroscopy. The structure has been solved at 200 and 100 K by single-crystal X-ray analysis. It crystallizes in the trigonal space group $P\bar{3}c1$ with $Z = 2$ Fe(II) units at both temperatures. The molecular structure consists of chains running along the *c* axis in which the Fe(II) ions are linked by three *N*4,*N*4′ coordinating bis(tetrazole) ligands. The main difference between the two forms appears to be in the Fe−N bond lengths, which are 2.164(4) Å at 200 K and 2.038(4) Å at 100 K. The Fe−Fe separations are 7.422(1) Å at 200 K and 7.273(1) Å at 100 K. The EXAFS results are consistent with the crystal structure. In both spin states, the FeN_6 octahedron is almost regular within the EXAFS resolution. The Fe−N distance is found as 2.16(2) Å at 300 K and 2.00(2) Å at 40 K. The absence of the "7 Å peak" in the EXAFS spectra of $[Fe(btzp)_3](ClO_4)_2$, in contrast with what has been observed for the $[Fe(4\text{-R-}1,2,4\text{-triazole})_3](anion)_2$ chain compounds, confirms that this peak can be used as the signature of a metal alignment only when it involves a strongly enhanced multiple scattering M−M−M path, with M−M spacing less than 4 Å. Irradiation with green light at 5 K has led to the population of the metastable high-spin state for the iron(II) ion. The nature of the spin-crossover behavior has been discussed on the basis of the structural features.

Introduction

A challenging field of research concerns the study of bistable molecular systems.[1] A spectacular example of molecular bistability is provided by the phenomenon of spin crossover (SC).[2−6] One of the goals is to design new materials exhibiting spin-crossover behavior characterized by sharp spin transitions accompanied by thermal hysteresis, as well as an associated thermochromic effect.[3,7−10] Such a behavior has been observed in some mononuclear Fe(II) compounds.[6,11−17] The archetype of such compounds is $[Fe(1\text{-propyltetrazole})_6](BF_4)_2$;[6,18−19] the

[†] Johannes Gutenberg University.
[‡] Institut de Chimie de la Matière Condensée de Bordeaux.
[§] Utrecht University.
[||] Leiden University.
[⊥] Université Paris XII-Val de Marne.
[▽] Université Paris Sud.

(1) Kahn, O.; Launay, J. P. *Chemtronics* **1988**, *3*, 140.
(2) Gütlich, P. *Struct. Bond.* **1981**, *44*, 83.
(3) Zarembowitch, J.; Kahn, O. *New J. Chem.* **1991**, *15*, 181.
(4) Kahn, O. *Molecular Magnetism*; VCH Publishers: New York, 1993.
(5) König, E. *Prog. Inorg. Chem.* **1987**, *35*, 527.
(6) (a) Gütlich, P.; Hauser, A. *Coord. Chem. Rev.* **1990**, *97*, 1. (b) Gütlich, P.; Hauser, A.; Spiering, H. *Angew. Chem., Int. Ed. Engl.* **1994**, *33*, 2024. (c) Gütlich, P.; Jung., J.; Goodwin, H. A. *NATO ASI Ser. C* **1996**, *321*, 327. (d) Gütlich, P. *Mol. Cryst. Liq. Cryst.* **1997**, *305*, 17.
(7) Kahn, O.; Codjovi, E. *Philos. Trans. R. Soc. London A* **1996**, *354*, 359.
(8) Kahn, O.; Codjovi, E.; Garcia, Y.; van Koningsbruggen, P. J.; Lapouyade, R.; Sommier, L. In *Molecule-Based Magnetic Materials*; Turnbull, M. M., Sugimoto, T., Thompson, L. K., Eds.; ACS Symposium Series 644; American Chemical Society: Washington, DC, 1996; p 298.
(9) Kröber, J.; Codjovi, E.; Kahn, O.; Grolière, F.; Jay, C. *J. Am. Chem. Soc.* **1993**, *115*, 9810.
(10) Kahn, O.; Kröber, J.; Jay, C. *Adv. Mater.* **1992**, *4*, 718.
(11) (a) Sylva, R. N.; Goodwin, H. A. *Aust. J. Chem.* **1967**, *20*, 479. (b) Ritter, G.; König, E.; Irler, W.; Goodwin, H. A. *Inorg. Chem.* **1978**, *17*, 224.
(12) Sorai, M.; Ensling, J.; Hasselbach, K. M.; Gütlich, P. *Chem. Phys.* **1977**, *20*, 197.
(13) (a) Hutchinson, B. B.; Daniels, L.; Henderson, E.; Neill, P.; Long, G. J.; Becker, L. W. *J. Chem. Soc., Chem. Commun.* **1979**, 1003. (b) Grandjean, F.; Long, G. J.; Hutchinson, B. B.; Ohlhausen, L.; Neill, P.; Holcomb, J. D. *Inorg. Chem.* **1989**, *28*, 4406.
(14) König, E.; Ritter, G.; Kulshreshtha, S. K.; Castary, N. *Inorg. Chem.* **1984**, *23*, 1903.
(15) (a) Buchen, T.; Gütlich, P:, Sugiyarto, K. H.; Goodwin, H. A. *Chem.−Eur. J.* **1996**, *2*, 1134. (b) Sugiyarto, K. H.; Weitner, K.; Craig, D. C.; Goodwin, H. A. *Aust. J. Chem.* **1997**, *50*, 869.

10.1021/ic991118n CCC: $19.00
Published on Web 04/04/2000

hysteresis is due to a first-order crystallographic phase transition.[20] Strong intermolecular interactions, resulting from the presence of an important hydrogen-bonding network[12,15] or extended $\pi-\pi$ interactions,[16,17] were also invoked to be responsible for the occurrence of thermal hysteresis. Mononuclear Fe(II) compounds exhibiting these features are rather scarce, and the requirements for such physical behavior are most difficult, if not impossible, to control. A more straightforward strategy toward cooperative SC compounds is represented by the use of potentially bridging ligands.[21] In this way, the ligand establishes the communication between the active SC sites. The driving force for the SC process is the gain in entropy, which is predominantly vibrational in origin. In a polynuclear crystal lattice, the molecular distortions involved in the low-spin (LS) to high-spin (HS) transition may efficiently be spread through the whole crystal lattice via the ligands linking the SC sites. The cooperativity may even be enhanced by hydrogen-bonding interactions within the crystal lattice. The mechanism describing this cooperativity is not yet fully understood; however, one of the most heuristic explanations is probably provided by the model developed by Spiering et al., which is based on elastic interactions.[22]

Up to now, few polymeric Fe(II) SC materials were reported. This polymeric strategy involves either 4-substituted-1,2,4-triazole derivatives or ligands based on N-donating heterocyclic groups linked by a spacer. The SC compounds of the former class are represented by the linear chain compounds of formula $[Fe(4\text{-R-trz})_3](anion)_2 \cdot xH_2O$ (4-R-trz = 4-substituted-1,2,4-triazole).[12,7−10,23−27] The direct linkage of the Fe(II) centers by triple *N*1,*N*2-1,2,4-triazole bridges was assumed to account for the cooperative nature of the SC. The use of these materials in molecular electronics for data processing is currently being investigated.[4,10,28]

The latter class of ligands was designed in order to investigate the synergy between the dimensionality of the Fe(II) SC compounds and their physical behavior. $[Fe(1,2\text{-di-}(4\text{-pyridyl})\text{-ethylene})_2(NCS)_2]$ is the first catenane supramolecular SC compound; however, the spin conversion is rather gradual.[29] On the other hand, the following two-dimensional systems display cooperative SC behavior with thermal hysteresis: $[Fe\{N(entz)_3\}_2](anion)_2$ ($N(entz)_3$ = tris[(tetrazol-1-yl)ethane]-amine; anion = BF_4^-, ClO_4^-)[30] and $[Fe(btr)_2(NCX)_2]$ (btr = 4,4′-bis-1,2,4-triazole; X = S[31] or Se[32]). The latter system consists of layers of six-coordinate Fe(II) ions linked in the equatorial plane by single bridges of the btr ligand via the *N*1 atoms. The NCX^- anions are coordinated in trans positions. Using the noncoordinating anions BF_4^- and ClO_4^-, the first Fe(II) SC molecular materials with a three-dimensional network have been obtained. For instance, $[Fe(btr)_3](ClO_4)_2$ shows an unusual two-step spin conversion, related to the presence of iron(II) ions in two crystallographically inequivalent sites.[33]

Our approach consists of applying the linkage of the tetrazole moieties by alkyl groups in order to obtain polynuclear Fe(II) SC materials. It is well-known that 1-alkyl-substituted tetrazoles yield mononuclear Fe(II) compounds showing SC behavior.[6,18,34−40] In this paper, we report on $[Fe(btzp)_3](ClO_4)_2$ where btzp stands for 1,2-bis(tetrazol-1-yl)propane, schematized as

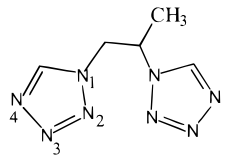

We will first describe the crystal structure, at both 200 and 100 K, and then we will investigate the magnetic and Mössbauer properties. We will show that the compound presents the light-induced excited spin state trapping effect (LIESST). This paper will also include an EXAFS study. This technique has been proved to be particularly useful to obtain structural information on Fe(II) polymeric SC compounds. In particular, it was found that, in the $[Fe(4\text{-R-1,2,4-trz})_3](anion)_2$ compounds, the metal ions were aligned with Fe−Fe intrachain separations close to 3.5 Å.[41] Therefore, it was necessary to provide a structural tool

(16) (a) Letard, J. F.; Guionneau, P.; Codjovi, E.; Lavastre, O.; Bravic, G.; Chasseau, D.; Kahn, O. *J. Am. Chem. Soc.* **1997**, *119*, 10861. (b) Letard, J. F.; Guionneau, P.; Rabardel, L.; Howard, J. A. K.; Goeta, A. E.; Chasseau, D.; Kahn, O. *Inorg. Chem.* **1998**, *37*, 4432.
(17) Zhong, Z. J.; Tao, J. Q.; Yu, Z.; Dun, C. Y.; Liu, Y. J.; You, X. Z. *J. Chem. Soc., Dalton Trans.* **1998**, 327.
(18) (a) Franke, P. L.; Haasnoot, J. G.; Zuur, A. P. *Inorg. Chim. Acta* **1982**, *59*, 5. (b) Müller, W. E.; Ensling, J.; Spiering, H.; Gütlich, P. *Inorg. Chem.* **1983**, *22*, 2074.
(19) Wiehl, L. *Acta Crystallogr.* **1993**, *B49*, 289.
(20) Jung, J.; Schmitt, G.; Wiehl, L.; Hauser, A.; Knorr, K.; Spiering, H.; Gütlich, P. *Z. Phys. B* **1996**, *100*, 523.
(21) Kahn, O.; Garcia, Y.; Letard, J. F.; Mathonière, C. *NATO ASI Ser. C* **1998**, *518*, 127.
(22) (a) Sanner, I.; Meissner, E.; Köppen, H.; Spiering, H. *Chem. Phys.* **1984**, *86*, 227. (b) Willenbacher, N.; Spiering, H. *J. Phys. C: Solid State Phys.* **1988**, *21*, 1423. (c) Spiering, H.; Willenbacher, N. *J. Phys.: Condens. Matter* **1989**, *1*, 10089.
(23) (a) Lavrenova, L. G.; Ikorskii, V. N.; Varnek, V. A.; Oglezneva, I. M.; Larionov, S. V. *Koord. Khim.* **1986**, *12*, 207. (b) Lavrenova, L. G.; Ikorskii, V. N.; Varnek, V. A.; Oglezneva, I. M.; Larionov, S. V. *Koord. Khim.* **1990**, *16*, 654. (c) Lavrenova, L. G.; Yudina, N. G.; Ikorskii, V. N.; Varnek, V. A.; Oglezneva, I. M.; Larionov, S. V. *Polyhedron* **1995**, *14*, 1333.
(24) Codjovi, E.; Sommier, L.; Kahn, O.; Jay, C. *New J. Chem.* **1996**, *20*, 503.
(25) (a) Garcia, Y.; van Koningsbruggen, P. J.; Codjovi, E.; Lapouyade, R.; Kahn, O.; Rabardel, L. *J. Mater. Chem.* **1997**, *7*, 857. (b) Garcia, Y.; van Koningsbruggen, P. J.; Lapouyade, R.; Fournès, L.; Rabardel, L.; Kahn, O.; Ksenofontov, V.; Levchenko, G.; Gütlich, P. *Chem. Mater.* **1998**, *10*, 2426.
(26) van Koningsbruggen, P. J.; Garcia, Y.; Codjovi, E.; Lapouyade, R.; Kahn, O.; Fournès, L.; Rabardel, L. *J. Mater. Chem.* **1997**, *7*, 2069.
(27) Garcia, Y.; van Koningsbruggen, P. J.; Lapouyade, R.; Rabardel, L.; Kahn, O.; Wieczorek, M.; Bronisz, R.; Ciunik, Z.; Rudolf, M. F. *C. R. Acad. Sci. Paris* **1998**, *II c*, 523.
(28) Jay, C.; Grolière, F.; Kahn, O.; Kröber, J. *Mol. Cryst. Liq. Cryst.* **1993**, *234*, 255.
(29) Real, J. A.; Andrés, E.; Munoz, M. C.; Julve, M.; Granier, T.; Bousseksou, A.; Varret, F. *Science* **1995**, *268*, 265.
(30) (a) Bronisz, R.; Ciunik, Z.; Drabent, K.; Rudolf, M. F. *Conference Proceedings, ICAME-95* **1996**, *50*, 15. (b) Bronisz, R. Ph.D. thesis, University of Wroclaw (Poland), 1999.
(31) (a) Vreugdenhil, W.; Haasnoot, J. G.; Kahn, O.; Thuéry, P.; Reedijk, J. *J. Am. Chem. Soc.* **1987**, *109*, 5272. (b) Vreugdenhil, W.; van Diemen, J. H.; de Graaff, R. A. G.; Haasnoot, J. G.; Reedijk, J.; van der Kraan, A. M.; Kahn, O.; Zarembowitch, J. *Polyhedron* **1990**, *9*, 2971.
(32) Ozarowski, A.; Shunzhong, Y.; McGarvey, B. R.; Mislankar, A.; Drake, J. E. *Inorg. Chem.* **1991**, *30*, 3167.
(33) Garcia, Y.; Kahn, O.; Rabardel, L.; Chansou, B.; Salmon, L.; Tuchagues, J. P. *Inorg. Chem.* **1999**, *38*, 4663.
(34) Poganiuch, P.; Gütlich P. *Hyperfine Interact.* **1988**, *40*, 331.
(35) Adler, P.; Poganiuch, P.; Spiering, H. *Hyperfine Interact.* **1989**, *52*, 47.
(36) Poganiuch, P.; Decurtins, S.; Gütlich, P. *J. Am. Chem. Soc.* **1990**, *112*, 3270.
(37) Gütlich, P.; Poganiuch, P. *Angew. Chem., Int. Ed. Engl.* **1991**, *30* (8), 975.
(38) Buchen, T.; Gütlich, P. *Chem. Phys. Lett.* **1994**, *220*, 262.
(39) Buchen, T.; Poganiuch, P.; Gütlich, P. *J. Chem. Soc., Dalton Trans.* **1994**, 2285.
(40) Hinek, R.; Spiering, H.; Schollmeyer, D.; Gütlich, P.; Hauser, A. *Chem.—Eur. J.* **1996**, *2*, 1127.
(41) (a) Michalowicz, A.; Moscovici, J.; Ducourant, B.; Cracco, D.; Kahn, O. *Chem. Mater.* **1995**, *7*, 1833. (b) Michalowicz, A.; Moscovici, J.; Kahn, O. *J. Phys. IV* **1997**, *7*, 633. (c) Michalowicz, A.; Moscovici, J.; Garcia, Y.; Kahn, O. *J. Synchrotron Radiat.* **1999**, *6*, 231.

able to detect directly the signature of this metal alignment. This was done by EXAFS using the signature of a multiple scattering signal lying at the double Fe−Fe distance, the so-called "7 Å peak". For the present compound, the EXAFS study was not absolutely necessary since it has been possible to grow single crystals suitable for X-ray diffraction. Nevertheless, we decided to perform EXAFS measurements in order to study how the amplitude of the 7 Å multiple scattering peak varies when the metal−metal separation is modified.

Experimental Section

Physical Measurements. Elemental analyses were performed by the Service Central d'Analyse (CNRS) in Vernaison, France. Infrared spectra were carried out with a Perkin-Elmer Paragon 1000 FT-IR spectrophotometer using KBr pellets. Magnetic susceptibilities were measured in the temperature range 300−5 K with a fully automated Manics DSM-8 susceptometer equipped with a TBT continuous-flow cryostat and a Drusch EAF 16 UE electromagnet operating at ca. 1.7 T. Data were corrected for magnetization of the sample holder and for diamagnetic contributions, which were estimated from the Pascal constants.[57]Fe Mössbauer measurements were performed using a constant acceleration Halder-type spectrometer with a room temperature ^{57}Co source (Rh matrix) in transmission geometry. All isomer shifts reported in this work refer to natural iron at room temperature. The spectra were fitted to the sum of Lorentzians by a least-squares refinement. For the LIESST experiments, ca. 20 mg of the polycrystalline compound was placed in a disk-shaped polished PMMA container (ca. 3 cm^2 surface) and mounted in a helium cryostat for temperature variation between 4 and 300 K. The sample was irradiated at 5 K with an argon ion laser (514 nm, 25 mW cm^{-2}) for 20 min within the cavity of the Mössbauer spectrometer. The spectra were then fitted to Lorentzians with the program MOSFUN[42] assuming equal Debye−Waller factors to the HS and LS state at a given temperature. The EXAFS spectra were recorded at LURE, the French synchrotron radiation facility, on the storage ring DCI (1.85 GeV, 300 mA), on the EXAFS13 spectrometer, with a Si111 channel-cut monochromator. The detectors were low-pressure (≈0.2 atm) air-filled ionization chambers. Each spectrum is the sum of three recordings in the range 7090−8090 eV, including the iron K-edge (≈7115 eV). The spectra were recorded at room temperature and 40 K with a liquid helium cryostat. The samples were prepared as homogeneous compressed pellets with a mass (about 50 mg) calculated in order to obtain an absorption jump at the edge $\Delta\mu x \approx 1.0$ with a total absorption above the edge less than $\mu x \approx 2$. The EXAFS data analysis was performed with the "EXAFS pour le Mac" and EXAFS98 programs[43] on an Apple Macintosh personal computer. This standard EXAFS analysis[44] includes linear pre-edge background removal, polynomial and cubic spline atomic absorption calculation, Lengeler−Einsenberger EXAFS spectra normalization,[45] and reduction from the absorption data $\mu(E)$ to the EXAFS spectrum $\chi(k)$ with $k = \{[2m_e/(\tilde{n}h^2)]$ where E_0 is the energy threshold, taken at the absorption maximum (7125 ± 1 eV). Radial distribution functions $F(R)$ were calculated by Fourier transforms of $k^3w(k)\mu(k)$ in the range 2−14 Å^{-1}; $w(k)$ is a Kaiser−Bessel apodization window with a smoothness coefficient $\tau = 3$. After Fourier filtering, the first single shell Fe-6N is fitted, in the range 3−14 Å^{-1} (resolution $\pi/2\partial k = 0.14$ Å), to the standard EXAFS formula, without multiple scattering:

$$k_\chi(k) = -S_0^2\left[\frac{N}{R^2}|f(\pi,k)|\, e^{-2\sigma^2k^2}\, e^{-2R/[\lambda(k)]} \times \sin(2kR + 2\partial_1(k) + \psi(k))\right] \quad (1)$$

where S_0^2 is the inelastic reduction factor and N is the number of nitrogen atoms at a distance R from the copper center. $\lambda(k) = k/\Gamma$ is the mean free path of the photoelectron. σ is the Debye−Waller coefficient, characteristic of the width of the Fe−N distance distribution. $\partial_1(k)$ is the central atom phase shift; $|f(\pi,k)|$ and $\psi(k)$ are the amplitude and phase of the nitrogen backscattering factor. Spherical-wave theoretical amplitudes and phase shifts calculated by the code FEFF were used.[46] Since the theoretical phase shifts were utilized, it is necessary to fit the energy threshold E_0 by adding an extra fitting parameter, ΔE_0. In the low-temperature spectrum, it was also necessary to introduce two Fe−N distances, at 2 and 2.18 Å. This is why the EXAFS is represented by a sum of two terms, reflecting the mixing of both LS and HS states, even at 40 K. The goodness of fit is given by $\rho(\%) = \sum[k\chi_{exp}(k) - k\chi_{th}(k)]^2/\sum[k\chi_{exp}(k)]^2$ and the error bars are estimated in the standard manner, using the statistical $\Delta\chi^2$.[44c] The experimental error bars were estimated by the method proposed by Vlaic.[47] For this statistical evaluation, the EXAFS spectrum at 300 K was chosen; this spectrum is the noisiest. Its average signal was found to be equal to 0.14 and the corresponding average standard deviation to 0.015; thus, the signal/noise ratio is close to 10. The choice between equivalent models was guided by an EXAFS version of the statistical F-test.[48] Since the crystal structure of the studied compound has been solved, it was possible to perform a modeling of the whole spectrum by an ab initio calculation using all the atoms lying around the central iron(II) ion within a sphere of 8 Å, in order to include at least one shell of two iron neighbors belonging to the Fe chain. This theoretical calculation was performed with the ab initio modeling program FEFF7.[46] The atomic coordinates were directly taken from the crystal structures. The molecular modifications introduced in the model before FEFF calculations were carried out with the molecular modeling program CHEM3D, and the user interface between CHEM3D, the crystal structure, and the FEFF inputs was significantly helped by the new utility, CRYSTALFF.[49]

Starting Materials. Commercially available solvents, sodium azide, triethyl orthoformate, 1,2-diaminopropane, ascorbic acid, iron(II) perchlorate hexahydrate, and iron(II) tetrafluoroborate hexahydrate were used without further purification. The 1,2-diaminopropane contains an asymmetric carbon atom; the racemic mixture was used.

Synthesis of 1,2-Bis(tetrazol-1-yl)propane (btzp). The ligand btzp was prepared from sodium azide, triethyl orthoformate, and 1,2-diaminopropane according to the general method described by Kamiya and Saito.[50] Yield: 73%. Anal. Calcd for $C_5H_8N_8$: C, 33.33; H, 4.48; N, 62.19. Found: C, 33.43; H, 4.67; N, 52.55. The high nitrogen content gives rise to particular difficulties in the determination of the elemental analysis.

Syntheses of $[Fe(btzp)_3](ClO_4)_2$. The compound was prepared as follows: 1 mmol (0.36 g) of $Fe(ClO_4)_2\cdot 6H_2O$ and 5 mg of ascorbic acid dissolved in 30 mL of ethanol were added to 3.21 mmol (0.54 g) of btzp dissolved in 10 mL of ethanol. After 2 days, the compound crystallized upon slow evaporation of the solvent at room temperature. Colorless crystals were collected and dried under ambient air. Yield: 73%. Anal. Calcd for $C_{15}H_{24}Cl_2O_8FeN_{24}$: C, 22.65; H, 3.04; N, 42.27; Fe, 7.02. Found: C, 22.88; H, 3.01; N, 42.20; Fe, 7.49. IR (ClO_4^-): $\nu_1 = 625$ cm^{-1} and $\nu_2 = 1100$ cm^{-1}.

(42) Müller, E. W. Ph.D. Thesis, 1982, University of Mainz, Germany.
(43) (a) Michalowicz, A. In *Logiciels pour la Chimie*; Société Française de Chimie: Paris, **1991**; p 102. (b) Michalowicz, A. *J. Phys. IV* **1997**, *7*, 235.
(44) (a) Teo, B. K. In *Inorganic Chemistry Concepts, EXAFS: Basic Priciples and Data Analysis*; Springer-Verlag: Berlin, 1986; p 9. (b) Königsberger, D. C.; Prins, R. *X-Ray Absorption Principles, Applications, Techniques of EXAFS, SEXAFS and XANES*; John Wiley: New York, 1988. (c) Lytle, F. W., Sayers, D. E., Stern, E. A., Co-Chairmen Report of the International Worshop on Standards and Criteria in X-Ray Absorption Spectroscopy. *Physica* **1989**, *B158*, 701.
(45) Lengeler, B.; Eisenberger, P. *Phys. Rev.* **1980**, *B21*, 4507.
(46) (a) Rehr, J. J.; Zabinsky, S. I.; Albers, R. C. *Phys. Rev. Lett.* **1992**, *69*, 3397. (b) Rehr, J. J. *Jpn. J. Appl. Phys.* **1993**, *32*, 8. (c) Rehr, J. J.; Mustre de Léon, J.; Zabinsky, S. I.; Albers, R. C. *J. Am. Chem. Soc.* **1991**, *113*, 5135. (d) Mustre de Leon, J.; Rehr, J. J.; Zabinsky, S. I.; Albers, R. C. *Phys. Rev.* **1991**, *B44*, 4146. (e) Rehr, J. J.; Albers, R. C. *Phys. Rev.* **1990**, *B41*, 8139.
(47) Vlaic, G.; Andreatta, D.; Cepparo, A.; Cepparo, P. E.; Fonda, E.; Michalowicz, A. *J. Synchrotron Radiat.* **1999**, *6*, 225.
(48) (a) Michalowicz, A.; Provost, K.; Laruelle, S.; Mimouni, A.; Vlaic, G. *J. Synchrotron Radiat.* **1999**, *6*, 233. (b) Joyner, R. W.; Martin, K. J.; Meehan, P. J. *J. Phys. C* **1987**, *20*, 4005.
(49) Provost, K.; Michalowicz, A. Unpublished software.
(50) Kamiya, T.; Saito, Y. Ger. Offen. **1973**, 2147023.

Table 1. Crystallographic Data for $[Fe(btzp)_3](ClO_4)_2$ at 100 and 200 K

formula	$C_{30}H_{48}FeN_{48}Cl_4O_{16}$	$C_{30}H_{48}FeN_{48}Cl_4O_{16}$
mol wt	1590.5	1590.5
cryst syst	trigonal	trigonal
space group	*P*3*c*1 (No. 165)	*P*3*c*1 (No. 165)
a, *b* (Å)	11.030(2)	11.098(2)
c (Å)	14.546(2)	14.844(2)
V (Å^3)	1532.6(4)	1583.3(5)
Z	2	2
T (K)	100	200
λ (Å)	0.71073	0.71073
ρ_{calc} (g/cm^3)	1.7233(4)	1.6681(5)
μ (Mo Kα, cm^{-1})	7.5	7.3
$R(F)^a$	0.050	0.052
$R_w(F^2)^a$	0.128	0.121

[a] $R(F) = \sum||F_o| - |F_c||/\sum|F_o|$ for $F_o > 4\sigma(F_o)$, $R_w(F^2) = [\sum w(F_o^2 - F_c^2)^2/\sum wF_o^2]^{1/2}$, $w = 1/(\sigma^2(F_o^2) + 0.035F^2)$, $F = (F_o + 2F_c)/3$.

Table 2. Fe−Fe Distance and Selected Bond Lengths (Å) for $[Fe(btzp)_3](ClO_4)_2$ (Esd's in Parentheses)[a]

	$T = 100$ K	$T = 200$ K
Fe−Fe	7.273(1)	7.422(1)
Fe−N4	2.038(4)	2.164(4)
N1−N2	1.332(8)	1.33(1)
N1−C1	1.304(8)	1.290(8)
N1−C2	1.448(9)	1.44(1)
N2−N3	1.276(7)	1.273(9)
N3−N4	1.367(7)	1.345(8)
N4−N1	1.292(6)	1.294(7)
C2−C3	1.32(2)	1.34(2)
C2−C2[a]	1.437(6)	1.406(6)

[a] C2[a] is generated by the symmetry operation *y*, *x*, 0.5 − *z*.

Table 3. Selected Bond Angles (deg) for $[Fe(btzp)_3](ClO_4)_2$ at 100 and 200 K (Esd's in Parentheses)[a]

	$T = 100$ K	$T = 200$ K
N4−Fe−N4[b]	90.8(2)	91.1(2)
N4−Fe−N4[c]	90.8(2)	91.1(2)
N4−Fe−N4[d]	180	180
N4−Fe−N4[e]	89.2(2)	88.9(2)
N4−Fe−N4[f]	89.2(2)	88.9(2)
Fe−N4−N3	122.7(3)	122.1(3)
Fe−N4−C1	132.0(4)	131.8(4)

[a] Atoms marked with a letter are generated by symmetry operations: (b) $-y, x-y, z$; (c) $-x+y, -x, z$; (d) $-x, -y, -z$; (e) $y, -x+y, -z$; (f) $x-y, x, -z$.

Crystal Structure Determination. A single crystal of dimensions 0.2 × 0.3 × 0.3 mm was mounted in a Lindemann-glass capillary and transferred into the cold nitrogen stream on an Enraf-Nonius CAD4-T diffractometer on a rotating anode. The structure was solved by automated direct methods (SHELXS-86). Refinement on F^2 was carried out using full-matrix least-squares techniques (SHELXL-97). Neutral atom scattering factors and anomalous dispersion corrections were taken from the *International Tables for Crystallography*. Geometrical calculations and illustrations were performed with PLATON. Crystal data as well as details of the data collection and refinement procedure are given in Table 1. Selected bond lengths and angles at 100 and 200 K are given in Tables 2 and 3.

Results

Description of the Structure. A view of the cationic iron(II) linear chain is depicted in Figure 1. The space group at 100 and 200 K is $P\bar{3}c1$. The asymmetric unit consists of an iron(II) ion and one half of the btzp ligand. The C3 of the 1,2-propane linkage is crystallographically disordered; the occupancy adds to 1 for the two disordered positions. A disordered perchlorate anion completes this asymmetric unit. The Cl−O bond lies along a 3-fold axis. Therefore, the three oxygen atoms are crystallographically related. The Fe(II) ion lies on the 3-fold inversion axis $\bar{3}$ and has an inversion center. It is in an octahedral environment formed by six crystallographically related *N*4 coordinating 1-tetrazole moieties. The fairly perfect O_h symmetry for the FeN_6 core is therefore present in the HS and LS states. This *N*4 coordination of the 1-substituted tetrazole moiety is in agreement with the findings for the $[Fe(1\text{-alkyltetrazole})_6](anion)_2$ series.[19,40] The Fe−N4 distance of 2.164(4) Å at 200 K corresponds to the value expected for an Fe(II) ion in the HS state.[5] It is slightly shorter than the Fe−N4 distance of 2.180(3) Å found at 195 K for the mononuclear compound $[Fe(ptz)_6](BF_4)_2$.[19] At 100 K, the Fe−N4 distance is equal to 2.038(4) Å, which is a typical value for an Fe(II) ion in the LS state.[5] The Fe−N4 distance decreases by 6% upon the spin conversion, which corresponds to the values found for other spin-crossover compounds.[5] The Fe(II) octahedron is very slightly distorted in the HS state with two sets of bond angles N−Fe−N of 91.1(2)° and 88.9(2)°. However, as expected, it is quasi regular in the LS state with bond angles N−Fe−N of 90.8(2)° and 89.2(2)°. Such high symmetry for the HS Fe(II) state has also been found for the mononuclear compounds $[Fe(ptz)_6](anion)_2$ (anion = BF_4^-, ClO_4^-), which crystallize in the space group $R\bar{3}$.[19] The Fe(II) ions are linked by a bridge composed of three bis(tetrazole) ligands, leading to a regular linear chain running along the *c* axis with Fe−Fe separations of 7.422(1) Å at 200 K and 7.273(1) Å at 100 K, as depicted in Figure 1. The btzp ligand has a bent conformation, which is illustrated by the torsion angle N1−C1−C2[a]−N1[a] (a = *y*, *x*, 0.5 − *z*) of −34(1)° at 200 K and of −35(1)° at 100 K. A projection of the structure at 200 K perpendicular to the *c* axis is shown in Figure 2. The space filling of the Fe(II) chains shows a hexagonal motif. In turn, the linear chains are packed in such a way as to form hexagonal cavities in the *ab* plane. The noncoordinated perchlorate anions reside in the voids of this molecular architecture. There are no intermolecular contacts between the linear chains. The apparent contacts between C3 atoms originating from different chains may be attributed to the statistical disorder of these C3 atoms. Furthermore, the strong thermal coefficients associated with the oxygen atoms originating from the perchlorate anions reflect their partial delocalization, and these features already indicate that these anions are not maintained by significant molecular contacts within the crystal lattice. Indeed, these anions are not involved in any hydrogen-bonding interactions with the cationic chain. This is in sharp contrast with the

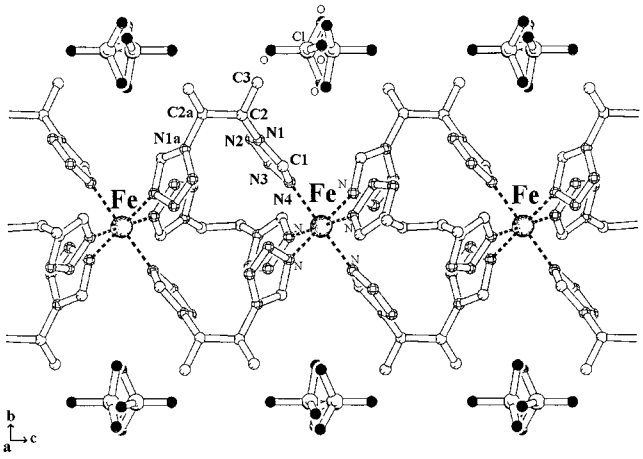

Figure 1. View of the structure of $[Fe(btzp)_3](ClO_4)_2$ along the *a* axis at 100 K.

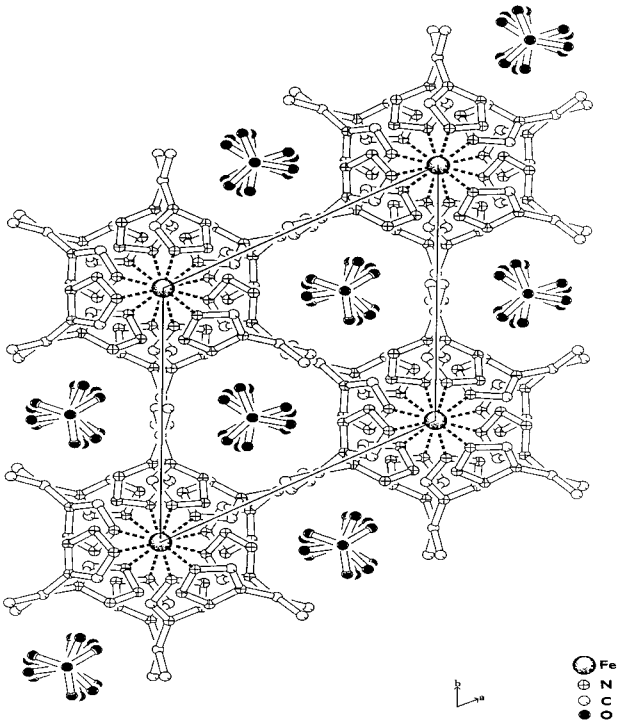

Figure 2. View of the structure of $[Fe(btzp)_3](ClO_4)_2$ along the *c* axis at 100 K.

crystal structure of $[Fe(btr)_3](ClO_4)_2$, where numerous CH···O contacts were detected between the ligands and the perchlorate anions.[33]

EXAFS Study. The experimental EXAFS spectra at 40 K (a) and at room temperature (b) and their Fourier transforms (c, d) are represented in Figure 3. The principal features are very similar to those of the spectra of polymeric Fe(II)−4-R-1,2,4-triazole compounds.[41,51] The first peak represents the FeN_6 octahedron, and its shift in position reflects the expected Fe−N distances increasing from the LS to the HS state. This peak was Fourier-filtered and fitted, as described in the Experimental Section, and the results are reported in Table 4.

In the HS state, the FeN_6 core is found to be a regular octahedron, in agreement with the crystallographic data. The EXAFS Fe−N distance, 2.18(2) Å, is slightly longer than that determined by X-ray diffraction, but the EXAFS spectrum was recorded at 300 K, and the crystal structure solved at 200 K. Compared to the values obtained in the LS state (0.08 versus 0.05 Å), the Debye−Waller factor significantly increased. This behavior can reflect either an increase of the thermal vibrations or a static distortion of the octahedron. The fit was not improved by adding a second Fe−N distance in order to take into account such a supposed distortion. Such a distortion, if any, is much smaller than the spectral resolution.

Contrary to the HS filtered spectrum at room temperature, that at 40 K cannot be fitted correctly with a single distance. The results displayed in Table 4 show that when a shell of Fe−N distances corresponding to the HS state is added (fit 2), the model is significantly improved compared to a model with 6 nitrogens at the same LS distance (fit 1). In order to avoid the so-called "mutiple solution trap" [52] due to parameter correlations, the two Fe−N distances were restrained to vary in a reasonable range, namely, 1.98−2.02 Å in the LS state and 2.16−2.20 Å in the HS state, and the two corresponding numbers of neighbors, N_1 and N_2, were constrained to obey the relation $N_1 + N_2 = 6$. Within these fitting conditions, it was found that the molar fraction of HS sites at 40 K is 0.20(5). This result is less accurate but in total agreement with the Mössbauer estimation.

In the present case, the most interesting EXAFS result concerns the medium-distance behavior. Several Fe(II), Ni(II), and Cu(II) polymeric compounds with 4-R-trz ligands were already studied by EXAFS.[41,51] In all cases, the metal−metal distance is close to 3.5 Å, and a peak around 7 Å, i.e., at the double distance, is observed. This may be valid at both low and room temperature, and in the case of Fe(II) in both the LS and HS states.[41] In the EXAFS spectra of the title compound, such a 7 Å peak is totally absent. This absence is pointed out in Figure 3, panels c and d, in which the position of the expected Fe−Fe signal (7.3−7.4 Å) is underlined by an arrow.

Figure 4 shows the theoretical $k\chi(k)$ spectra calculated with FEFF7. Curves a and b correspond to the LS and the HS state, respectively. These calculations were performed with the atomic coordinates extracted from the present crystal structures. These FEFF models are the first example of ab initio EXAFS calculations on an Fe(II) SC chain compound in both spin states. Except for one overall Debye−Waller factor ($\sigma^2 = 0.0049$ Å^2), identical for all the scattering paths, there are no fitted parameters. Although this choice leads to a slight amplitude misfit between theoretical and experimental $k\chi(k)$ curves (see Figure 3a,b), it is suitable to show how the structural changes accompanying the SC modify the EXAFS spectra. It should be noted that the only significant change revealed by the X-ray study is the Fe−N distances (2.0 → 2.16 Å). In both spin states, the FeN_6 octahedron remains regular and the structure of the ligand remains essentially unchanged. The comparison between experimental and theoretical $k\chi(k)$ is quite convincing. The changes of the relative amplitudes of the oscillation maxima (noted 1, 2, 3 and 4 in Figure 4) for the LS and HS spectra agree with those in the experimental ones, as shown in Figure 3a,b. One should notice that apparent amplitude variations induced by the SC (see, for instance, oscillation 2) are actually due to distance changes and interference effects between EXAFS oscillations.

Figure 5a presents the Fourier transform of the theoretical EXAFS spectrum in the LS state. In the input FEFF model, the Fe−Fe distance of 7.28 Å was not neglected a priori. The absence of the "7 Å peak" in the experimental spectra (see Figure 3c,d) is confirmed by the theoretical calculation. The only way to have an Fe−Fe peak at this distance is to add artificially an intermediate Fe(II) ion just in the middle of the actual Fe−Fe line in order to get an extra EXAFS signal corresponding to a multiple scattering path of the photoelectron. This multiple scattering enhancement is shown in Figure 5b.

Magnetic Properties. The magnetic behavior of $[Fe(btzp)_3](ClO_4)_2$ is shown in Figure 6 in the form of the $\chi_M T$ versus T plot, χ_M being the molar magnetic susceptibility per iron(II) ion and T the temperature. At 295 K, the $\chi_M T$ value is 3.626 cm^3 K mol^{-1}, which corresponds to what is expected for a HS iron(II) ion. Upon cooling, the $\chi_M T$ value remains constant until 200 K, after which it gradually decreases until 60 K. The $\chi_M T$ value of 0.760 cm^3 K mol^{-1} at 60 K corresponds to a mixture of LS and HS ions, with the molar fractions 0.80 and 0.20, respectively. Below 20 K, the $\chi_M T$ value slightly decreases, reaching a value of 0.528 cm^3 K mol^{-1} at 6 K. This decrease in the low-temperature range may be attributed to the zero-field splitting of the residual HS sites. The inversion temperature, $T_{1/2}$, where

(51) Garcia, Y.; van Koningsbruggen, P. J.; Bravic, G.; Guionneau, P.; Chasseau, D.; Cascarano, G. L.; Moscovici, J.; Lambert, K.; Michalowicz, A.; Kahn, O. *Inorg. Chem.* **1997**, *36*, 6357.
(52) Michalowicz, A.; Vlaic, G. *J. Synchrotron Radiat.* **1998**, *5*, 1317.

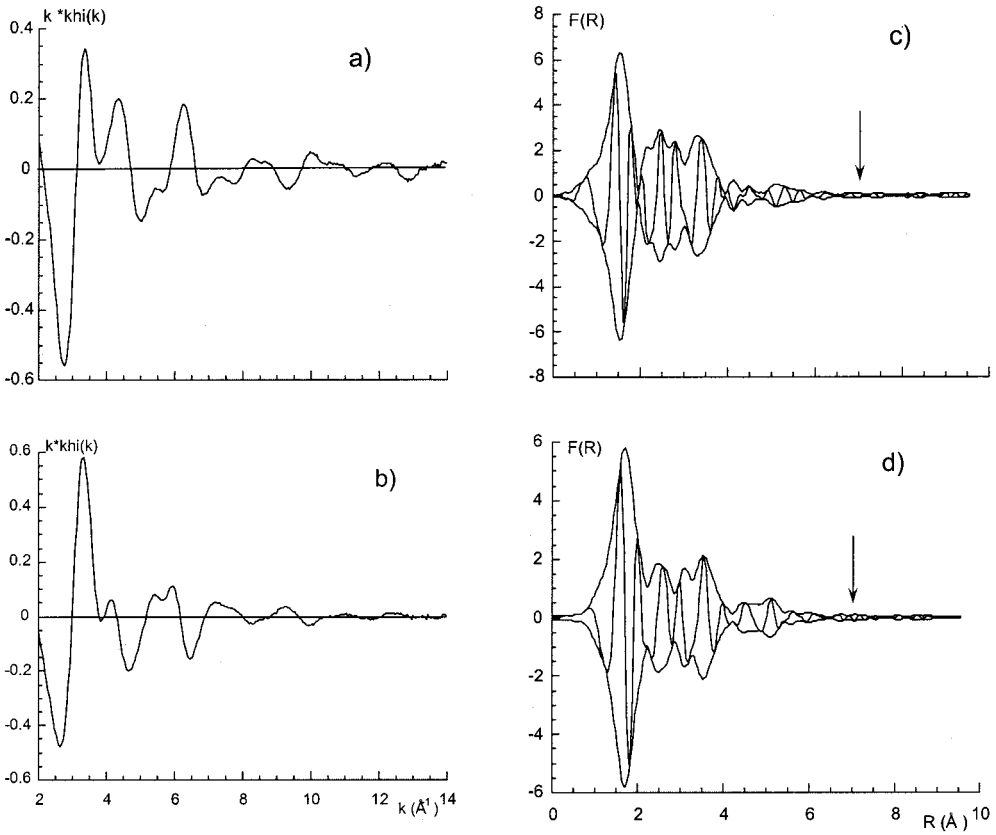

Figure 3. Experimental EXAFS spectra of $[Fe(btzp)_3](ClO_4)_2$: (a) $k\chi(k)$ spectrum in the LS state at 40 K; (b) $k\chi(k)$ spectrum in the HS state at 300 K; (c) Fourier transform (±modulus and imaginary part) at 40 K; (d) Fourier transform (±modulus and imaginary part) at 300 K.

Table 4. Fitting of the First Fe Coordination Sphere of the EXAFS Data for $[Fe(btzp)_3](ClO_4)_2$

	N	Γ (Å^{-2})	σ (Å)	R (Å)	ΔE_0 (eV)	ρ (%)
300 K one Fe−N distance	6.0[a]	0.92(1)	0.08(1)	2.18(1)	−0.7(5)	0.5
40 K one Fe−N distance	6.0[a]	0.92[a]	0.10(1)	2.03(2)	0.9(10)	8.0
40 K two shell fit $N_1 + N_2 = 6.0$	4.8(3) 1.2(3)	0.92[a] id	0.05(1) 0.08(2)	2.00(3) 2.18(2)	1.2(1.0) −1.0(1.0)	0.6

[a] Fixed values.

the molar fractions of LS and HS sites are both equal to 0.5, is found as 130 K. The transition does not show any hysteresis, since the $\chi_M T$ versus T curves recorded at decreasing and increasing temperatures are identical.

Figure 6 also shows the γ_{HS} versus T curve; the HS molar fraction, γ_{HS}, is deduced from the magnetic susceptibility through

$$\gamma_{HS} = (\chi_M T)/(\chi_M T)_{HS} \quad (2)$$

where the $\chi_M T$ value in the HS state, $(\chi_M T)_{HS}$, is taken as 3.63 cm^3 K mol^{-1}. If we assume that the 20% of HS sites below 70 K are not involved in the SC process, then it is possible to simulate the SC curve, using the equation (eq 3) derived from the regular solution model.

$$\ln[(1 - \gamma_{HS})/\gamma_{HS}] = [\Delta H + \Gamma(1 - 2\gamma_{HS})]/RT - \Delta S/R \quad (3)$$

In eq 3, R is the gas constant, ΔH is the enthalpy variation, ΔS is the entropy variation associated with the SC, and Γ is the interaction parameter.[4] Least-squares fitting leads to $\Delta H = 6.2$ kJ mol^{-1}, $\Delta S = 45$ J K^{-1} mol^{-1}, and a Γ value smaller than 0.2 kJ mol^{-1}. The SC may be considered as being almost noncooperative.

Mössbauer Measurements. ^{57}Fe Mössbauer spectra were recorded as a function of temperature from 300 K down to 10 K. Theoretical spectra were fitted to the experimental ones using the MOSFUN program for Lorentzian resonance lines.[42] Representative spectra taken at six different temperatures are shown in Figure 7. The corresponding parameter values derived from the fitting procedure are listed in Table 5. Figure 7 also shows the theoretical subspectra for the HS and LS states. The room temperature spectrum could be fitted to two quadrupole doublets with isomer shift and quadrupole splitting values typical for iron(II) in the HS state (cf. Table 5). In agreement with the magnetic susceptibility measurements (cf. Figure 6), the compound exhibits pure HS behavior at room temperature; no Mössbauer signal is seen that refers to the LS state. On cooling, the low-velocity components of the spectrum dominate more and more over the high-velocity resonances. This is due to the spin transition from HS to LS, whereby the iron(II) LS resonance appears to be a broadened singlet, which overlaps with the low-velocity components of the HS doublets. At 10 K, there are still HS resonances left in the spectrum, with an area fraction of ca. 20%, indicating that the spin transition is not complete at the low-temperature end, which is also confirmed by the magnetic measurements.

LIESST Experiments. The sample was irradiated at 5 K with green light while mounted in the sample holder of the cryostat. Figure 8 shows the Mössbauer spectra recorded at 5 K before and after irradiation, and at 125 K after irradiation and thermal relaxation. The corresponding Mössbauer data derived from the spectral fitting procedure are collected in Table 5. At 5 K, before light irradiation, the spectrum reveals an area fraction of 76%

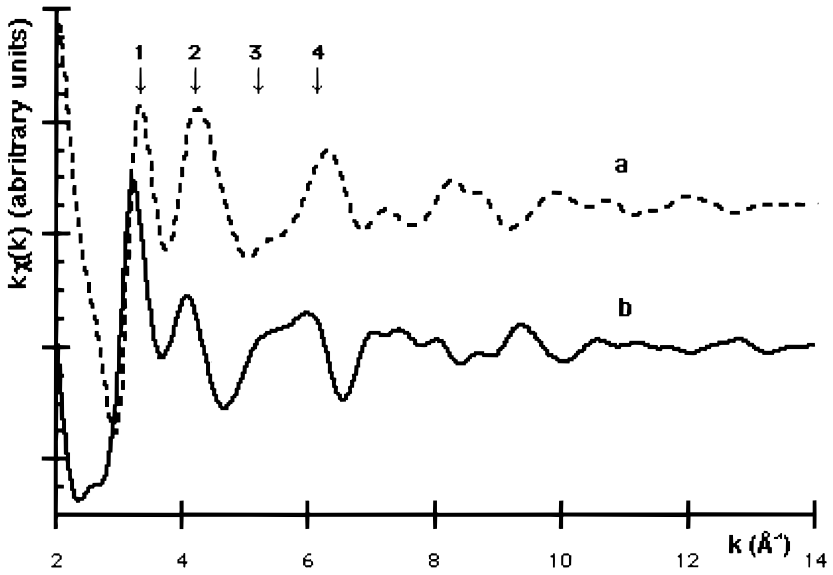

Figure 4. FEFF simulated spectra of $[Fe(btzp)_3](ClO_4)_2$ based on the crystal structures: (a) LS state and (b) HS state.

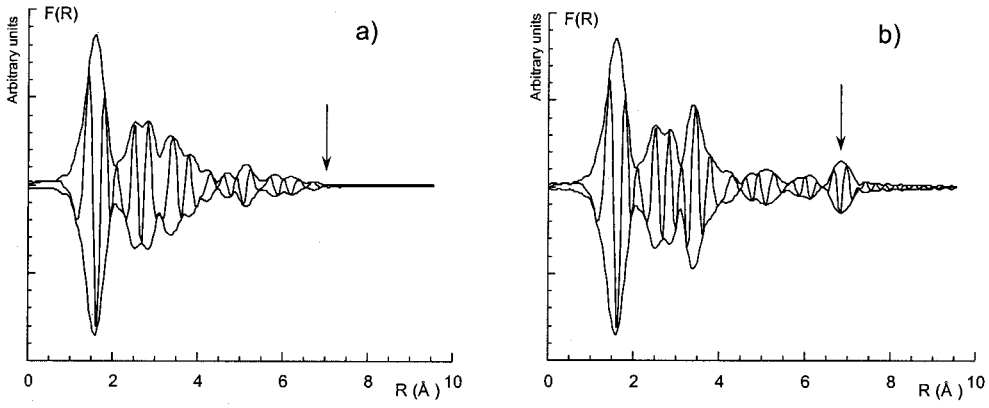

Figure 5. (a) Fourier transform of the FEFF model for the LS crystal structure of $[Fe(btzp)_3](ClO_4)_2$. (b) Same model with one extra Fe(II) ion placed in the middle of the actual Fe−Fe line.

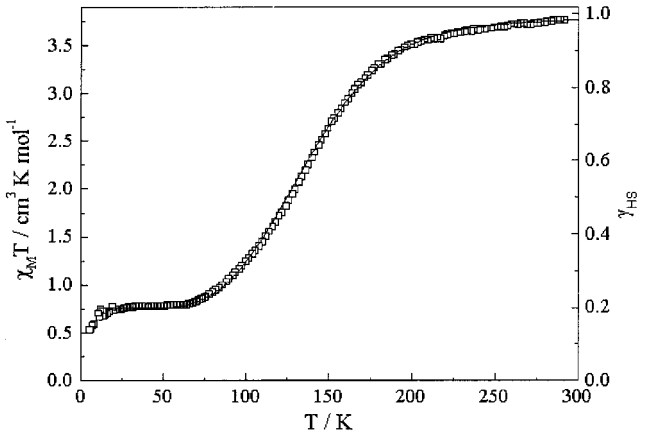

Figure 6. $\chi_M T$ and γ_{HS} versus T plots both in the cooling and warming modes for $[Fe(btzp)_3](ClO_4)_2$ in the 4.2−300 K temperature range.

for the LS sites and a total of 24% for the two HS sites. Through light irradiation, a considerable LS → HS conversion was observed. The area fractions of the resonance lines are now 91% for the HS and 9% for the LS state. Again, the HS ions were found to be distributed over two sites with a relative population of 44% and 47%, respectively. Upon warming the sample up to 20 K, 60% of the HS sites were found to have relaxed to the LS state. The thermal relaxation seems to take place with different velocities for the two HS sites. Above 50 K, the relaxation is complete. Figure 8 shows the spectrum recorded at 125 K after LIESST to prove the absence of decomposition through light irradiation. More quantitative investigation of the apparently complicated relaxation kinetics of the LIESST states was beyond the scope of this work, but will be pursued in later studies.

Discussion

$[Fe(btzp)_3](ClO_4)_2$ is the first one-dimensional Fe(II) SC material the structure of which was determined through X-ray diffraction. The synthetic strategy applied using the linkage of the tetrazole moieties by alkyl groups has indeed yielded a novel polynuclear Fe(II) SC compound. Rudolf et al. independently used this strategy with the tridentate ligand tris[(tetrazol-1-yl)-ethane]amine leading to a two-dimensional system.[30] In all these polynuclear Fe(II) tetrazole compounds, the ligand coordinates via the *N*4, as has also been found for the mononuclear hexakis-(1-alkyltetrazole) Fe(II) compounds.[19,40] The structure of $[Fe(btzp)_3](ClO_4)_2$ consists of triply bis(tetrazole-*N*4)-bridged Fe(II) chains. The linearity of the chains is preserved for both spin states. As in the mononuclear Fe(II) 1-alkyltetrazole compounds, the symmetry about the Fe(II) is that of a very regular octahedron, which is also reflected by the practically absent quadrupole splittings observed for the LS state in the ^{57}Fe Mössbauer spectra. Iron(II) in the LS state has practically no valence electron contribution to the electric field gradient.

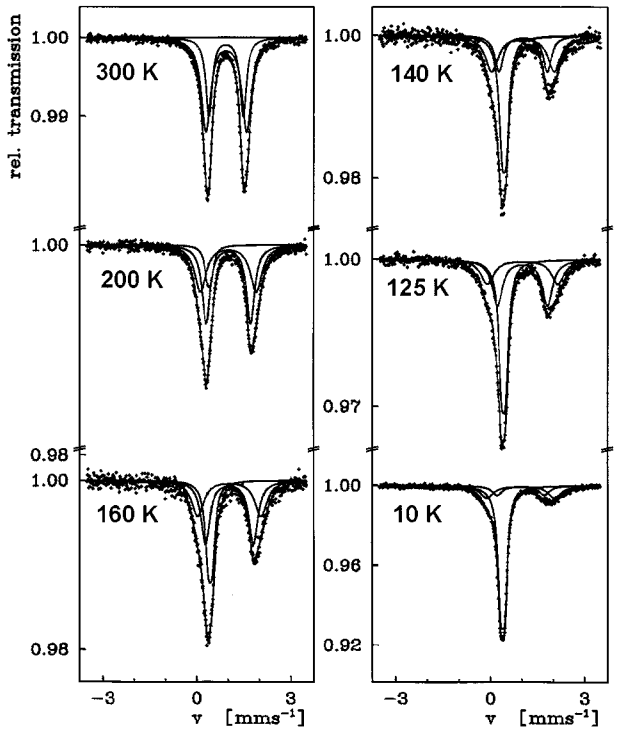

Figure 7. ^{57}Fe Mössbauer spectra for $[Fe(btzp)_3](ClO_4)_2$ at some selected temperatures.

Therefore, if the nearby lattice surroundings are practically cubic as in the present case, there is also no lattice contribution to the electric field gradient and no quadrupole splitting should be observed. This is the case for the LS state in the present study.

The bent conformation of the btzp ligand with torsion angle N1−C1−C2^a-N1^a (a = y, x, 0.5 − z) of −34(1)° at 200 K and of −35(1)° at 100 K is related to the dimensionality of the coordination compound formed. At first sight, it may seem to be surprising that the use of a ligand having two tetrazole moieties linked by an ethyl spacer leads to the formation of a chain, whereas the use of related ligands having other heterocyclic units yielded compounds of higher dimensionality.[29,53,54] The formation of the present linear chain structure is probably due to the particular arrangement of the tetrazole groups in syn conformation. Within this family of compounds, the only spin-crossover system is $[Fe(1,2\text{-di}(4\text{-pyridyl})ethylene)_2(NCS)_2]$, in which the Fe−Fe separation is as long as 13.66 Å.[29] The Fe−Fe separation in the present linear chain is only 7.422(1) Å at 200 K and 7.273(1) Å at 100 K.

$[Fe(btzp)_3](ClO_4)_2$ exhibits a gradual and incomplete spin transition, with $T_{1/2}$ = 130 K, which was followed by magnetic susceptibility measurements and ^{57}Fe Mössbauer spectroscopy. The residual HS fraction at lower temperatures (21% at 10 K) may be explained by the presence of crystal defects, such as chains of different lengths which cannot be detected by X-ray analysis. A comparison with the transition temperatures for the mononuclear compounds is rather tedious since the SC characteristics of compounds with different alkyl substituents on the tetrazole heavily depend on the crystal structure features. The transitions may be abrupt or rather gradual, and the $T_{1/2}$ values lie in the range 63−204 K.[18,34−40]

As seen in the X-ray structure, the methyl substituent of the ligand is distributed over two positions. Therefore, one can expect a distribution of several iron(II) sites, which most probably is the reason for the line broadening observed in the Mössbauer spectra.

The compound $[Fe(btzp)_3](BF_4)_2$ was also prepared using strictly the same synthetic procedure as for the perchlorate derivative. It is isostructural with $[Fe(btzp)_3](ClO_4)_2$ and displays similar SC behavior, with $T_{1/2}$ shifted by 20 K toward higher temperatures. This increase of $T_{1/2}$ with the decrease of the size of the noncoordinating anion is in line with the quasi linear relationship found between $T_{1/2}$ and the radius of the spherical anions, which has been observed for the linear chain compounds $[Fe(4\text{-R-trz})_3](anion)_2$,[27,55] as well as for $Co^{II}(2,2':6',2''\text{-terpyridine})_2](anion)_2$.[56] A further systematic study of the variation of the anion in these btzp materials would be required to check whether this tendency is equally valid for spherical anions.

The very gradual character of the SC and the absence of hysteresis deserve to be discussed further. Thus, although $[Fe(btzp)_3](ClO_4)_2$ has a polymeric structure, the SC process appears to be almost noncooperative. The interaction parameter in the ideal solution model, Γ,[57] was found to be smaller than 0.2 kJ mol^{-1}. The threshold value above which a thermal hysteresis could be expected would be 2.3 kJ mol^{-1}. Several factors may be responsible for this behavior. The X-ray crystal structure analysis revealed the absence of a hydrogen-bonding network. Besides, in spite of the direct linkage of the active spin-crossover sites by triple bis(tetrazole) bridges, these centers are rather far apart, about 7.3 Å. This value roughly corresponds to the double Fe−Fe distance found by EXAFS spectroscopy in $[Fe(4\text{-R-trz})_3](anion)_2$ chain compounds.[41] As these latter compounds generally show cooperative spin transitions, one may conclude that the spacing of the Fe(II) ions in the present structure does not favor an effective propagation of the cooperativity along the chain. This explanation, however, is to our experience not very likely. Normally one should expect a higher degree of cooperativity as the spin state changing iron centers get closer together, with the consequence that changes in the phonon system and elastic interactions due to spin transition can be communicated more effectively to nearby iron centers rather than more distant ones. The SC behavior observed for $[Fe(btzp)_3](ClO_4)_2$ may be compared to the one obtained by metallic dilution in $[Fe(4\text{-R-trz})_3](anion)_2$.[29,58] In these diluted materials, the active sites are statistically more spaced in comparison to the pure compound. The transitions become smoother as the percentage of doping increases. In the present btzp compound, the Fe−Fe separation is directly imposed by the crystal structure. However, the key factor determining the quasi absence of cooperativity seems to be the nature of the linkage between the Fe(II) ions rather than the Fe−Fe separation. The 1,2-propane spacer between the two tetrazole moieties is rather flexible and may act as a shock absorber against the elastic interactions between Fe(II) ions, which are at the origin of cooperativity. This situation contrasts with that encountered in $[Fe(4\text{-R-trz})_3](anion)_2$ compounds in which the *N*1,*N*2-1,2,4-triazole linkage is very rigid, and allows an excellent transmission of the intersite interactions.

(53) Garcia, Y.; van Konisbruggen, P. J.; Kooijman, H.; Haasnoot, J. G.; Spek, A. L.; Kahn, O. *Eur. J. Inorg. Chem.* **2000**, 307.
(54) Wu, L. P.; Yamagiwa, Y.; Kuroda-Sowa, T.; Kamikawa, T., Munakata, M. *Inorg. Chim. Acta* **1997**, *256*, 155
(55) Varnek, V. A.; Lavrenova, L. G. *J. Struct. Chem.* **1994**, *35*, 842.
(56) Figgis, B. N.; Kucharski, E. S.; White, A. H. *Aust. J. Chem.* **1983**, *36*, 1537.
(57) Schlichter, C. P.; Drickamer, H. G. *J. Chem. Phys.* **1972**, *56*, 2142.
(58) (a) Lavrenova, L. G.; Ikorskii, V. N.; Varnek, V. A.; Oglezneva, I. M.; Larionov, S. V. *J. Struct. Chem.* **1993**, *34*, 960. (b) Shvedenkov, Y. G.; Ikorskii, V. N.; Lavrenova, L. G.; Drebushchak, V. A.; Yudina, N. G. *J. Struct. Chem.* **1997**, *38*, 579. (c) Varnek, V. A.; Lavrenova, L. G. *J. Struct. Chem.* **1997**, *38*, 850.

Table 5. ^{57}Fe Mössbauer Parameters[a] (mm s^{-1}) for $[Fe(btzp)_3](ClO_4)_2$ before and after Irradiation (LIESST)

T (K)	δ (LS)	ΔE_Q (LS)	Γ (LS)	A_{LS} (%)	δ (HS)	ΔE_Q (HS)	Γ (HS)	A_{HS} (%)	δ (HS)	ΔE_Q (HS)	Γ (HS)	A_{HS} (%)
300				0	0.94(0)	1.30(3)	0.20(2)	59	0.93(0)	1.11(0)	0.12(1)	41
200	0.39(1)	0.11(2)	0.11(1)	11	1.01(0)	1.78(6)	0.22(1)	41	1.01(0)	1.42(2)	0.15(1)	48
160	0.42(1)	0.12(1)	0.11(1)	29	1.04(1)	2.02(7)	0.22(3)	36	1.04(1)	1.54(3)	0.16(2)	35
140	0.43(1)	0.13(1)	0.12(1)	43	1.04(1)	1.99(5)	0.25(2)	33	1.04(1)	1.54(3)	0.16(2)	24
125	0.42(0)	0.13(1)	0.13(1)	44	1.02(1)	2.24(4)	0.25(2)	26	1.02(1)	1.59(2)	0.20(2)	30
10	0.52(0)	0.14(0)	0.11(0)	79	1.07(1)	2.30(3)	0.25(2)	16	1.06(1)	1.60(4)	0.20(2)	5
5	0.53(0)	0.14(0)	0.11(0)	80	1.07(1)	2.30(3)	0.25(2)	16	1.06(1)	1.60(4)	0.20(2)	4
						After LIESST						
5	0.53(1)	0.14(1)	0.12(1)	9	1.07(1)	2.30(2)	0.23(1)	44	1.05(1)	1.70(2)	0.20(1)	47

[a] δ = isomer shift, ΔE_Q = quadrupole splitting, $\Gamma/2$ = half-width of the lines, A_{HS} = area fraction of the HS doublets. Statistical standard deviations are given in parentheses.

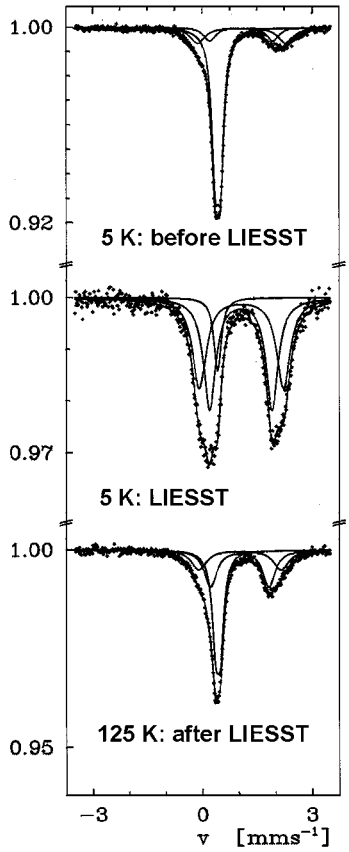

Figure 8. LIESST effect observed by Mössbauer spectroscopy: (top) at 5 K, with light irradiation; (middle) at 5 K, after light irradiation; (bottom) at 125 K, after light irradiation.

Upon going from the HS to LS state, the main structural changes are observed in the Fe−N distances, which are 2.164(4) Å at 200 K and 2.038(4) Å at 100 K. Interestingly, this modification is not particularly reflected by the conformation of the ligand, which is illustrated by the small deviations in the torsion angle N1−C1−C2^a-N1^a (a = y, x, 0.5 − z) of −34(1)° at 200 K and −35(1)° at 100 K. Clearly, the change in the Fe−N distance is not compensated by any other noticeable effect, except the increase in the Fe−Fe separation. Indeed, the largest change in cell dimensions, 2.1%, was found for the *c* axis, i.e., the chain axis. The changes in the *a* and *b* axes are considerably smaller (0.6%). The actual cell volume decreases by 3.3% upon going from 200 to 100 K. The volume change per Fe(II) ion is 25.4 Å^3, which falls in the range normally observed.[5] The regularity of the FeN_6 octahedron, even in the HS state, deserves to be discussed. The electronic ground state of a HS Fe(II) ion in an octahedral symmetry is $^5T_2$, and a Jahn−Teller distortion might be anticipated. Such a distortion was observed in many cases.[19,40] In the present work, neither X-ray diffraction nor EXAFS can detect any octahedron distortion. However, the Debye−Waller factor deduced from the EXAFS data increases from the LS to the HS state ($\Delta\sigma^2 = 0.0039$ Å^2). This Debye−Waller variation is essentially due to a change in the Fe−N vibrational properties; it is well established that Fe−N bonds are higher in the HS state than in the LS state and Fe−N stretching frequencies are lower in the HS state than in the LS state.[59,60]

The absence of any Fe−Fe signature at 7.3 Å definitely demonstrates the Fe−Fe−Fe multiple scattering nature of such a peak observed in polymeric $[Fe(4\text{-R-trz})_3](anion)_2$ compounds with a shorter Fe−Fe separation.[41,51] The present work confirms that there are no parasitic multiple scattering signals due to the carbon and nitrogen atoms of the ligands; the "7 Å peak" is observed only in aligned M−M−M structures with M−M spacing less than 4 Å and involves a double metal−metal distance in order to undergo the so-called multiple scattering enhancement effect.

The Mössbauer spectra reveal the typical quadrupole doublets with characteristic parameter values for iron(II) in the HS state. As pointed out above, the structural analysis, both by X-ray diffraction and EXAFS, does not detect any noticeable distortion from regular octahedral symmetry around the iron centers. This implies that, in the present case of FeN_6 cores, one should not expect any significant lattice contribution to the electric field gradient at the iron centers. Thus, the observed quadrupole splittings observed for the HS states can only arise from a noncubic valence electron contribution over the iron molecular orbitals. And this can only be the result of a Jahn−Teller distortion which is actually expected for a d^6 complex ion in the $^5T_2$ ground state. The distortion in the present case, however, is so small that it could not be observed in the structural analysis. For electric quadrupole splitting to be observed for an iron(II) HS complex, the octahedral distortion should be such that a splitting of the t_{2g} orbital subset occurs on the order of a few hundred wavenumbers at room temperature. The quadrupole splitting observed for the HS states in the present study is in the range of 1.2 mm s^{-1}. In view of the fact that the largest quadrupole splittings observed for iron(II) HS compounds are $\leq$4 mm s^{-1}, in cases where the doubly occupied d_{xy} orbital lies lowest corresponding to octahedral compression, we can conclude that in the present case we are dealing with a marginal octahedral elongation along the chain with the orbital doublet $\{|xz\rangle,|yz\rangle\}$ lowest. The quadrupole splittings ΔE_Q of the HS states show a pronounced temperature dependence: they increase with decreasing temperature, which is expected if the energy separation between the t_{2g} orbitals, split by Jahn−Teller

(59) Takemoto, J. H.; Hutchinson, B. *Inorg. Chem.* **1973**, *12*, 705.
(60) Takemoto, J. H.; Streusand, B.; Hutchinson, B. *Spetrochim. Acta Part A* **1974**, *30*, 827.

distortion, is on the order of thermal energy with increasing electronic population in the low-lying orbital doublet toward lower temperatures.

The Mössbauer resonance lines arising from the HS states as well as those from the LS state all are broadened; they are approximately twice the natural line width. The line broadening is essentially temperature independent, which rules out the spin transition rate falling into the Mössbauer time window as a possible origin. A plausible explanation for the line broadening, however, is the following. As already mentioned above, the methyl groups of the propane bridge can occupy either one of the two positions in each ligand. This can theoretically lead to 64 different lattice sites for an iron center. A distinction by X-ray diffraction is not possible, because the methyl group appears to be disordered. The fact that the HS resonance lines could be reasonably well fitted to only two doublets supports the assumption that all possible isomeric conformations are not equally occupied and/or they can be grouped into two assemblies, of approximately equal total weight, regarding their influences on the quadrupolar interaction energies.

$[Fe(btzp)_3](ClO_4)_2$ undergoes the LIESST effect. To the best of our knowledge, this is the first one-dimensional SC compound behaving this way. No LIESST effect could be observed with the $[Fe(4\text{-R-trz})_3](anion)_2$ compounds. The occurrence of the LIESST effect may be related to the quasi absence of cooperativity. As a matter of fact, it has been convincingly established in other cases that the LIESST becomes more likely as the SC is less cooperative.[61] It is evident from our present preliminary studies that the thermal decay of the LIESST states in the different lattice sites shows different relaxation kinetics. We are planning to look into this problem using Mössbauer spectroscopy on ^{57}Fe-enriched samples. Optical spectroscopy will not be suitable for this purpose, as the different HS states may not be distinguished because of the broad absorption lines.

Conclusion

Further research on this type of polytetrazole systems is currently being carried out. Variation in the synthetic route provides a solid basis for tuning the spin-crossover behavior by modifying the nature of the linkage, and thereby allowing a systematic tuning of the Fe−Fe separation. One of the objectives is represented by increasing the efficiency of communication between the active SC sites, which can be achieved by either intra- or interchain interactions. In order to increase the cooperativity between Fe(II) sites within the chain, a more rigid and/or conjugated linkage between the tetrazole moieties may be used. This will prevent the "shock-absorbing" properties invoked for the title compound. As far as the interchain interactions are concerned, the projection displayed in Figure 2 indicates that the SC chains could be put into contact through the substituents on the spacer. This could be realized by taking advantage of the tools used in supramolecular chemistry, such as extended hydrogen bonding networks, $\pi-\pi$ interactions, or steric interactions. Another objective deals with the investigation of the relation between the dimensionality of the designed systems and the SC properties. Preliminary results already showed that the increase of the spacer leads to compounds of higher dimensionality.[30b] We intend to further investigate the interdependence among SC properties, dimensionality, and structural features.

Acknowledgment. We are very grateful to the staffs of the linear accelerator and storage ring at LURE. We thank Dr. F. Bouamrane for his help in EXAFS data recording and Dr. R. Lapouyade for helpful discussions. This work was partly funded by the TMR Research Network ERB-FMRX-CT98-0199 entitled "Thermal and Optical Switching of Molecular Spin States (TOSS)" and by the Council for Chemical Sciences of the Netherlands Organization for Scientific Research (CW-NWO). P.G. wishes to thank the Fonds der Chemischen Industrie and the Materialwissenschafliches Forschungszentrum der Universität Mainz for financial support.

Supporting Information Available: An X-ray crystallographic file for $[Fe(btzp)_3](ClO_4)_2$ in CIF format. FEFF input file and ORTEP drawing. This material is available free of charge via the Internet at http://pubs.acs.org.

IC991118N

(61) Constant-Machado, H. Ph.D. Thesis, University of Paris VI (France), 1997.